Photoelectron spectroscopy and scanning tunneling microscopy studies of the initial growth of the Sm-on-Pt(100) interface

H. J. Venvik, C. Berg, A. Borg, and S. Raaen
Physics Department, University of Trondheim, Norges Tekniske Høgskole, N-7034 Trondheim, Norway
(Received 10 October 1995)

The Sm-on-Pt(100) overlayer system has been studied by photoelectron spectroscopy, scanning tunneling microscopy (STM), and low-energy electron diffraction (LEED) at room temperature. As Sm overlayers were evaporated onto the Pt(100)-hex-$R0.7°$ reconstructed single-crystal surface, the initial growth of the interface was studied. Photoelectron spectroscopy and LEED indicate that Sm and Pt has formed an intermixed, disordered phase in the surface. The Pt $4f$ core-level spectra indicate the existence of an unresolved surface component that disappears with Sm deposition. For all Sm coverages (0.3–20 Å), trivalent Sm was observed. Some divalent Sm was seen after ~20 Å Sm deposition, and was believed to stem from Sm atoms at the surface. LEED and STM show that Sm adsorption induces a local lifting of the hexagonal reconstruction. The first monolayer of the Sm-Pt compound grows as long (100–1000 Å), narrow (30–50 Å) islands directed along the direction of longest periodicity of the reconstructed structure. At the same time, the uncovered areas display the hexagonally reconstructed structure. The Sm-Pt islands are seen to be centered on the elevated ridges of the reconstruction. There are no indications of preferential nucleation centers, such as steps or defects. Two effects are discussed to contribute simultaneously to the observed island shape: (1) an anisotropic Sm diffusion, favoring diffusion along the reconstruction ridges, and (2) lifting of the reconstruction along the elevated ridges is the energetically favorable process, due to lower Pt-Pt coordination in these on-top sites. [S0163-1829(96)04024-6]

INTRODUCTION

Compounds and alloys based on the lanthanides exhibit a wide variety of physical properties such as, e.g., magnetism, superconductivity, valence fluctuations as well as heavy fermion behavior. Small changes in the electronic structure of lanthanide-based compounds may lead to quite distinct alterations in physical properties. In addition, such systems have considerable technological interest since they are being used in, e.g., microelectronic industry, in catalysis, and in strong permanent magnets. Sm may be of particular interest (together with Ce, Eu, Tm, and Yb) from a fundamental point of view since two different isoenergetic states may coexist. Relatively small changes in chemical environment may induce a change in the valence states,[1] which thus may be a very sensitive indicator of the evolution of a given Sm-metal substrate interface. For example, Sm is trivalent in the bulk of Sm metal, whereas the atoms at the surface are in their divalent state.[2,3]

There have in recent years been several reports that rare earths that were deposited at room temperature onto various substrates have a tendency to form interface alloys or mixed interfaces that may extend to several lattice spacings.[4–11] This is related to the anomalous high diffusion coefficients that exist for various elements in rare-earth matrices.[12] This phenomenon must be considered when investigating rare-earth overlayers. Previous studies of samarium overlayers on various substrates have concluded that Sm may be divalent, trivalent, or homogeneously mixed valent in interfaces.[8,13–21] The nature of the mixed valence, i.e., if it is heterogeneous (different valence at different sites) or homogeneous (noninteger valence at a given site), may be determined by the proximity of the low binding energy Sm $4f$ feature to the Fermi level in photoemission experiments. If the $4f$ level closest to the Fermi level is located further below the Fermi level than ~0.4 eV, the nature of the valency is heterogeneous, and if not, a situation of homogeneous mixed valence will occur.[22]

Pt surfaces have been extensively studied because of their catalytic properties.[23] Pt has a high $5d$ density of states near the Fermi level, and thus strong interactions between Sm and Pt may be expected. The (100) surface of Pt is one out of three (100) surfaces, the other two being Au(100) and Ir(100), which exhibit a hexagonal surface reconstruction.[24–28] For Au(100) and Pt(100), the surface structure has been shown to influence the growth of Au (Ref. 29) and Pt (Ref. 30) overlayers, respectively.

The most stable configuration of the Pt(100) surface is the hex-$R0.7°$ reconstruction, written $\left[\begin{smallmatrix} N & 1 \\ -1 & 5 \end{smallmatrix}\right]$, $N=12-14$, in matrix notation. This structure was recently characterized on atomic scale with scanning tunneling microscopy (STM).[31] The surface layer of the Pt(100) crystal consists of a close-packed hexagonal layer, which is rotated 0.7° with respect to the underlying—and less dense—square layer. The mismatch between the two layers gives rise to a range of atomic sites on the surface, varying from ''on-top'' to ''fourfold'' sites. As a result, rowlike structures appear in the $[N\ 1]$ direction. Interesting features should therefore be observed when studying both the structure and growth, and the electronic properties of a Sm/Pt(100) overlayer system.

In the present work we have employed photoemission spectroscopy and STM in order to obtain information on structure as well as electronic properties of the Sm on Pt(100) overlayer system in the low Sm coverage regime, from 0 to ~3 Å Sm for the STM experiments, and from 0 to

~20 Å Sm for the photoemission experiments. All experiments were performed with the sample at room temperature.

EXPERIMENT

Synchrotron photoemission experiments were carried out at Beamline 22 at MAX-lab, Lund University, Sweden. Using a modified Zeiss SX700 plane-grating monochromator in conjunction with a large hemispherical analyzer, a total experimental resolution of ~100 meV was obtained for energies in the range 126–160 eV. The UHV chamber of Beamline 22 is equipped with a conventional LEED (low-energy electron diffraction) instrument.

Complementary x-ray photoemission spectroscopy (XPS) experiments as well as evaporation rate calibrations were made in the home laboratory. The XPS spectra were recorded using a HA-50 hemispherical electron energy analyzer from Vacuum Science Workshop (VSW) in conjunction with a twin-anode x-ray source (VSW), yielding an instrumental resolution of 1 eV.

The STM studies were performed in a separate home laboratory, with an UHV STM from Omicron Vacuumphysik GmbH. The STM measurements can be done at room temperature only, and the instrument is equipped with a tripod piezoscanner, allowing for a maximum scan range of 2000 Å×2000 Å. The probe tip was prepared from tungsten wire; the preparation and cleaning of tips are described elsewhere.[31] The STM measurements were carried out in the constant current mode, with 6.0-nA tunneling current and sample bias voltages in the range 3–100 mV. The sample was alternately positively and negatively biased, but this introduced no significant differences in the recorded images. The STM data are presented as top view, grey-scale images, with the darkest colors representing the lowest levels. No filtering routines were applied to the data. The STM laboratory also allows for standard LEED measurements.

The Pt(100) single crystal was cleaned by cycles of argon sputtering with the sample kept at either room temperature or ~350 °C, heating in oxygen (T~700 °C and 1×10^{-8} mbar), and annealing in vacuum (T~850 °C). After cleaning, the sample displays a very sharp LEED pattern and atomically resolved, high-quality STM images, the latter being very sensitive to surface contamination and irregularities. All measurements were performed on the same Pt(100) single crystal.

Sm was evaporated from a resistively heated tungsten basket, which had been thoroughly outgassed. The pressure during evaporation was $\sim1\times10^{-9}$ mbar. Due to different geometries, the deposition rates at the Pt(100) crystal surface differ for the three UHV systems. The deposition rate was estimated from evaporation of Sm on clean Ta, which is considered to be a noninteracting substrate, by monitoring the attenuation of the substrate core level. For the synchrotron photoemission and XPS experiments the deposition rate was estimated at ~2.0 Å/min, while Sm was deposited at a rate of ~0.15 Å/min in the STM studies. During the photoemission experiments the cleanliness of the sample was verified by monitoring O 1s and C 1s core-level emission. Oxygen and carbon could not be detected for low Sm coverages (<4.5 Å). Traces of oxygen and carbon were found at higher coverages, especially after repeated evaporations. Both evaporation and measurements were done with the sample at room temperature.

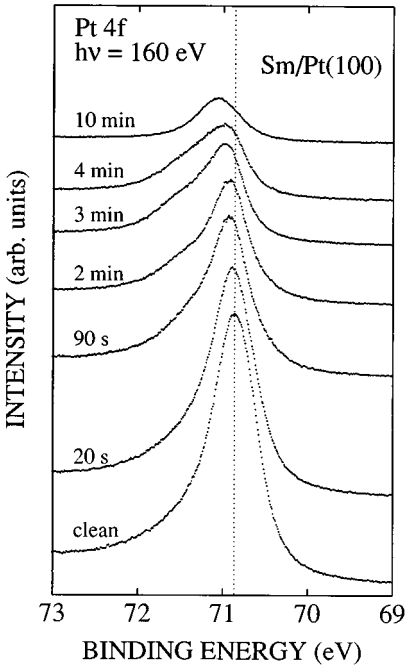

FIG. 1. Pt 4f photoelectron spectra from Pt(100) that has been exposed to Sm as indicated. The Sm evaporation rate was estimated at ~2.0 Å/min. The photon energy was 160 eV. The changes in peak shape and position indicate a reaction between Sm and Pt.

RESULTS AND DISCUSSION

A. LEED

With increasing Sm deposition, the LEED pattern of the hexagonal reconstruction gradually disappears, leaving only the (1×1) pattern for a Sm coverage of 2–3 Å. We therefore have a lifting of the reconstruction during the adsorption of approximately one Sm monolayer. Continued Sm deposition causes the (1×1) pattern to vanish as well. At a Sm coverage of 6–8 Å, all reflections are gone. This rapid disappearance of the LEED pattern indicates that the evolving surface is disordered.

B. Photoelectron spectroscopy

Figure 1 shows how the Pt 4f core-level spectrum develops as increasing amounts of Sm are evaporated onto the Pt(100) single crystal. The Sm evaporation rate was estimated at ~2.0 Å/min. The bottom curve is the signal from the clean crystal surface. As Sm is evaporated, a shoulder is seen to grow up at the high binding energy side of the Pt 4f peak. At the same time the position of the main peak shifts to higher binding energies. The change in peak shape and position bears evidence of a changed screening geometry around the Pt atoms in the surface. As the shoulder is seen to evolve with increasing Sm evaporation, it is interpreted to stem from Pt atoms that have reacted with Sm. The shoulder is quite broad, which may indicate many Pt-Sm coordinations. After a total of 10-min Sm deposition, only one broad peak is seen in the spectrum, positioned at 0.2 eV higher

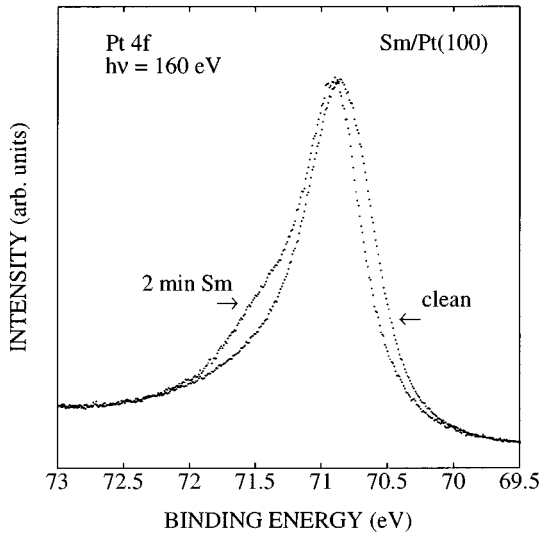

FIG. 2. A comparison of the Pt $4f$ spectra from the clean Pt(100)-hex-$R0.7°$ surface and the same surface after evaporation of Sm for 2 min at a rate estimated at ~2.0 Å/min. The shoulder at the high-binding-energy side of the peak stems from Pt atoms that has reacted with Sm, while the loss of intensity at the low-binding-energy side indicates an unresolved surface component in the spectrum of the clean sample. The spectra were recorded at a photon energy of 160 eV.

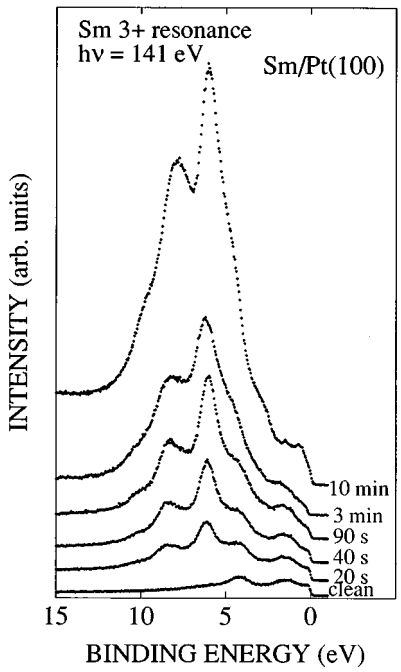

FIG. 3. The valence-band region recorded at the Sm 3+ resonance energy, with a photon energy of 141 eV. The bottom spectrum is the spectrum from a clean Pt sample, showing the Pt states in this region. As Sm is evaporated, two peaks are seen to grow up at 6 and 8.5 eV. They stem from Sm atoms in a trivalent state. The Sm evaporation rate was ~2.0 Å/min.

binding energy than the signal from the clean surface. This may correspond to a situation where all the Pt atoms in the surface have a more uniform Sm coordination. Electrons with kinetic energies ~100 eV have a mean free path of ~5 Å,[32] so the photoemission signal originates from the topmost atom layers. The fact that a Pt signal is observable after ~20 Å Sm evaporation indicates that Pt and Sm have formed an interface alloy that may extend a few layers into the surface.

A closer inspection of the peak shape reveals further information. Figure 2 shows a comparison between the signal from the clean Pt surface and the signal after 2 min (~4 Å) Sm evaporation. At this Sm coverage, no traces of the hexagonal reconstruction are seen with LEED, only the 1×1 structure. The observed shift in peak position is seen to start out as a loss of intensity at the low-binding-energy side of the Pt $4f$ peak at the same time as the shoulder appears at the high-binding-energy side. A corresponding intensity loss at the low-binding-energy side is observed in the Pt $4f$ signal as Pt(100) is exposed to CO.[33,34] We interpret this loss of intensity as originating from an unresolved surface component in the $4f$ spectrum of the Pt(100) surface. The surface component must stem from atoms in the hexagonally reconstructed surface having a slightly different energy than the Pt atoms in the bulk. The surface component is expected to be present only for surfaces with less than a monolayer Sm coverage. By subtracting the photoemission signal from a surface with submonolayer Sm coverage from the clean surface signal, a surface core-level shift (SCLS) of 0.1–0.2 eV to lower binding energy is found. Since the surface atoms sit in a range of different environments, this component is probably a sum of several contributions, which may explain why it is not resolved in our measurements.

In general, one expects that less dense surfaces show larger surface shifts. Pt(111) has the highest density of the unreconstructed single-crystal Pt surfaces, with the surface component being shifted -0.4 eV,[35] the negative sign indicating a shift to lower binding energies. The small SCLS of Pt(100)-hex-$R0.7°$ indicates that the atoms in the hexagonally reconstructed surface are more bulklike than atoms in the close-packed (111) surface. Similar trends in structure-dependent SCLS's have been seen for both Au (Refs. 36 and 37) and Ir (Ref. 38). Pt shows a larger difference between the close-packed (111) surface and the hexagonally reconstructed surface than both Ir(100)-(5×1) and Au(100)-(5×20). Possibly, the buckled structure of the surface reconstruction adds to the density in the surface, as discussed in Ref. 36.

To determine the valence state of Sm, we used the technique of resonant photoemission. The sample is excited with photons having energies that resonantly enhance emission from Sm $4f$ states through a Super-Coster-Kronig process.[39] Divalent and trivalent Sm have slightly different energies where the resonance has its maximum (135 and 141 eV, respectively). By tuning the photon energy between these maxima, the sensitivity for one of the valence states may be increased. Valence band spectra were also recorded a few eV below the resonances (''off''-resonance spectra). At this photon energy (126 eV) the valence-band spectra show mainly Pt states. Figures 3 and 4 show spectra recorded at the Sm 3+ and Sm 2+ resonance energies, respectively. An off-resonance spectrum (Fig. 4) and the spectrum from the clean surface (Fig. 3) are shown for comparison. As increasing amounts of Sm are deposited, Sm is seen to be trivalent (main peaks at 6.2- and 8.2-eV binding energy) for all Sm depositions. The 2+ resonance spectra in Fig. 4 show almost

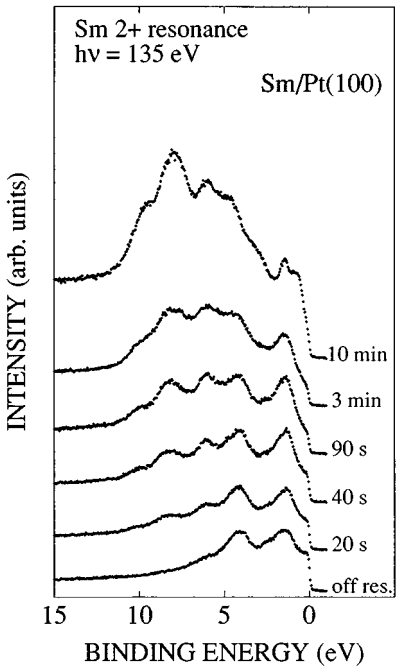

FIG. 4. Here the valence-band spectra are recorded at the Sm 2+ resonance energy (photon energy 135 eV), except for the bottom spectrum, which is recorded off the resonance energy (photon energy 126 eV). The off resonance spectrum shows mainly Pt states. As Sm is deposited onto the sample, weak signals (comparable to the Pt states) are seen at the 3+ position. After 10-min Sm evaporation, a 2+ doublet is seen to emerge close to the Fermi level. The Sm evaporation rate was ~2.0 Å/min.

the same features as the spectra recorded at the 3+ resonance (Fig. 3). This is partially due to the fact that the 3+ initial state will resonate slightly also at the 2+ resonance energy. But in addition no divalent Sm features can be observed for most Sm depositions. Only after 10 min Sm evaporation, a weak 2+ doublet peak at 0.5–1.5-eV binding energy can be seen to emerge. The 2+ peak position being further away from the Fermi level than 0.4 eV, as discussed in the Introduction, indicates that the mixed valence is heterogeneous in nature.

A reaction between Pt and Sm can be predicted from the Pt-Sm phase diagram,[40] which shows many Pt-Sm compounds, $SmPt_2$ and SmPt being the two most easily formed. Even though Sm-Pt compounds are expected to be trivalent in the bulk, the valence state of Sm atoms at the surface may not be so easily predicted. The Sm valence state is very sensitive to the chemical environment, such as, e.g., a surface, where Sm tends to be in its divalent state. Our data at low Sm coverages (i.e., <3 min evaporation time) show that Sm-Pt compounds or alloys that are formed in the interface are trivalent in the bulk as well as at the surface. The 2+ signal observed after 10 min Sm evaporation is believed to stem from Sm atoms on top of Sm in the surface, since we already have concluded that the Sm valence is heterogeneous, i.e., site dependent, and since the surface of Sm metal is divalent.

C. STM

Figure 5 shows ~0.15 Å of Sm deposited onto the hexagonally reconstructed Pt(100) surface. Long, narrow islands have evolved, while the uncovered areas display the hexagonally reconstructed structure. The islands are aligned along the direction of longest periodicity of the hexagonal reconstruction, the [N 1] direction. Islands with lengths varying from 100 Å up to 1000 Å are observed. After Sm deposition, single atoms on the surface can no longer be resolved. For this reason, the detailed atomic structure of the islands is difficult to determine. However, the images such as Fig. 6 strongly indicate that the island structures are disordered. Corrugation analysis of the STM data gives a value of 2.2 ±0.2 Å for the height of the islands with respect to the clean Pt substrate. The islands are seen to be centered on one single row in the hexagonal layer, covering this row and some of each neighboring row. The width of these rows is ~14 Å.[31] The direct measurement of the width of the islands

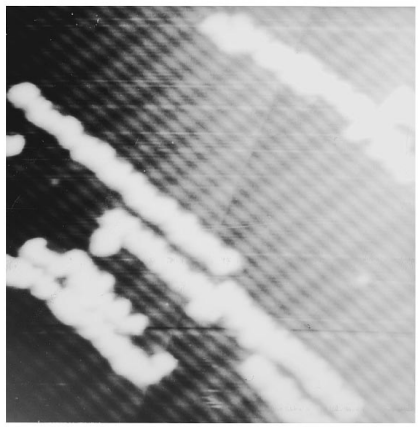

FIG. 5. The STM image shows 500 Å×500 Å of the hexagonally reconstructed Pt(100) surface after deposition of Sm for 1 min. The evaporation rate was estimated at ~0.15 Å/min. Long, narrow islands have evolved, while the uncovered areas still display the reconstructed structure. The islands are aligned along the direction of longest periodicity of the hexagonal reconstruction, the [N 1] direction. The grey scale covers 3.8 Å from black to white.

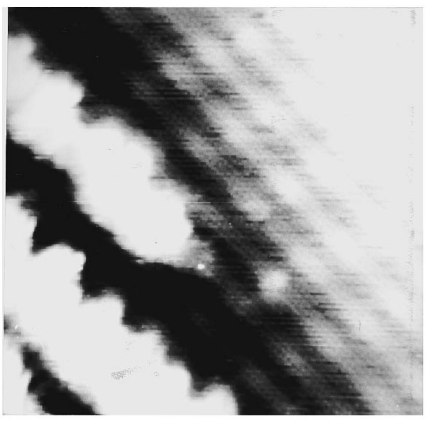

FIG. 6. A close up of 200 Å×200 Å of the Pt(100)-hex-R0.7° surface after 4 min Sm evaporation (~0.6 Å). While the reconstruction rows are resolved, no order can be seen in the Sm-Pt islands. The image also illustrates how the Sm-Pt islands grow centered along the elevated ridges of the reconstruction rows. The grey scale covers 2.5 Å from black to white.

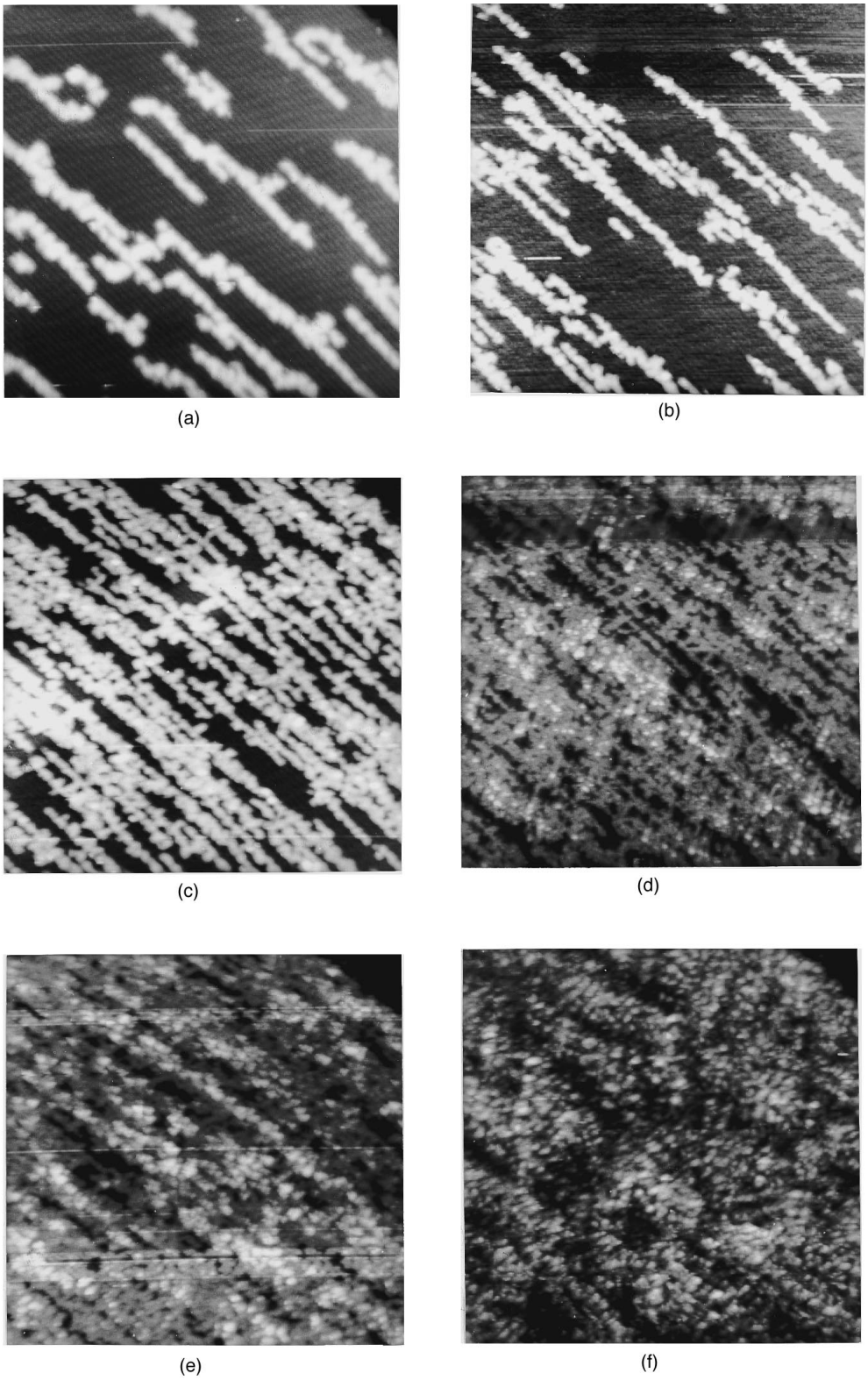

FIG. 7. Successive STM images (1000 Å×1000 Å) of the Pt(100) surface after 2 to 20 min of Sm evaporation. The estimated evaporation rate is 0.15 Å/min. (a) 2 min Sm (~0.3 Å), (b) 4 min Sm (~0.6 Å), (c) 8 min Sm (~1.2 Å), (d) 12 min Sm (~1.8 Å), (e) 16 min Sm (~2.4 Å), (f) 20 min Sm (~3.0 Å). After 8 min, the first appearance of a second layer is seen. Simultaneously, there are small, uncovered areas that still exhibit the hexagonal reconstruction. Some preferenced direction is still seen in the second layer after 16 min. After 20 min, the second layer is seen to consist of small, relatively isotropic islands.

from the recorded images here gives values of typically 30–50 Å. However, as the islands contain both Pt and Sm atoms and in addition are disordered, a width larger than 14 Å should probably be expected. However, we do not exclude that the island widths may be somewhat overestimated as a result of the character of the STM measurement. Also, the islands do not only follow one reconstruction row, both growth in the hexagonal $[-1\ 5]$ direction and occasional shifts of the center to neighboring rows are observed, as seen in Fig. 5.

Figure 7 shows a series of images, ranging from 2 to 20 min (~0.3 to ~3.0 Å) of Sm deposition. The adsorbed layer develops mainly in two dimensions. After 8 min of Sm deposition, the first appearance of a second layer is seen. Simul-

FIG. 8. Image of 600 Å×600 Å of the Pt(100) surface showing several steps perpendicular to the reconstruction rows. Sm has been evaporated for 1 min at an estimated rate of 0.15 Å/min. The step edges do not seem to act as nucleation centers for the Sm-Pt islands, as the islands are seen to have nucleated on both the lower terrace (lower right half of the figure) as well as at the steps (upper left corner).

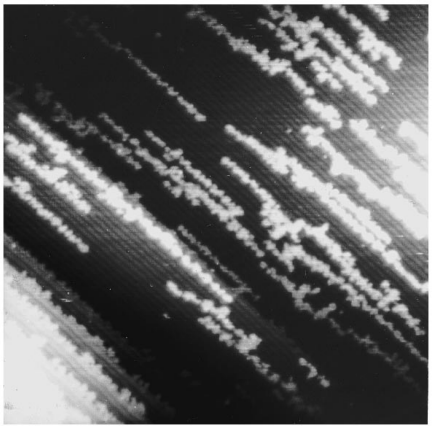

FIG. 9. STM image of an area of the reconstructed Pt(100) surface with steps running parallel to the reconstruction rows. The upper right half of the figure shows one large terrace (>750 Å wide), while the lower left corner shows one terrace with a width of ~250 Å and around seven narrow terraces (~40 Å wide). The Sm-Pt islands are seen to grow centered along the reconstruction rows and equally distributed on the flat terraces. A slight preference for nucleation at the step edges is also seen. The image covers 1000 Å×1000 Å, and estimated Sm exposure is ~0.6 Å.

taneously, there are small, uncovered areas that still exhibit the hexagonal reconstruction. The growth of the second layer proceeds in a different mode than the first layer. Although the Sm-Pt islands in the first layer are aligned along the $[N\ 1]$ direction, the surface disorder seems to be too large to affect the growth of the second layer appreciably. Some preference for island growth in the $[N\ 1]$ direction is seen in the second layer after 12 and 16 min Sm deposition. After 20 min, the second-layer islands are small, relatively isotropic, and evenly distributed. At this Sm coverage (~3 Å), the sample shows a slightly diffuse 1×1 LEED pattern.

Sm adsorption and growth on the Pt(100)-hex-R0.7° surface evidently induces a local lifting of the hexagonal reconstruction. The lifting of the hexagonal reconstruction induces space accommodation processes, since the hexagonal layer contains 20–25% more atoms than a square (1×1) layer. Thus Pt atoms in the uppermost, reconstructed layer can no longer fit into one single layer. Previous STM studies of gas adsorption (CO, O_2) on the same surface[31] showed that the transition to the (1×1) phase is initiated by nucleation of (1×1) islands on step edges more or less perpendicular to the reconstruction rows. Figure 8 shows that this is not the case in the Sm/Pt(100) system. Sm-Pt islands are seen to have nucleated both on a perfect terrace as well as at a step. Figure 9 shows a section of the surface with steps running along the reconstruction rows. On the lower, large terrace the islands seem to be equally distributed. A tendency of nucleation at the lower steps edges, still with islands growing along the $[N\ 1]$ direction, is observed. This step-edge adsorption is in correspondence with a prediction that generally the most favorable site of adsorption corresponds to the site where the atom has the highest coordination. Calculations for Pt on the Pt(111) surface[41] yield that the adsorption energy decreases from ternary to bridge and top sites. From this viewpoint only, one would expect that Sm would be found in the deep ''grooves'' of the surface reconstruction. However, we observe that the Sm-Pt islands are centered on the elevated ridges. It seems that it is not the Sm coordination, but rather the Pt-Pt coordination, that decides the position of the islands on the flat terraces. The activation energy for lifting the reconstruction appears to be lower for Pt atoms sitting on top of the elevated ridges of the reconstruction than for the fourfold coordinated Pt atoms in the ''grooves,'' the atoms sitting in top positions moving most easily out of the hexagonal layer. This leads to a growth rate that is different at different island edges, due to the Pt reconstruction. Such an effect was discussed in a study of Au on Au(100).[29] The growth of the (1×1) islands induced by gas adsorption was also seen to grow centered along the reconstruction rows,[31] as were the islands formed when Ni was deposited onto Au(100).[42] The centering may thus be seen in connection with transport of Pt atoms when the reconstruction is lifted. This constraint on the island growth influences the shape of the islands. In addition, the island shape may also reflect an anisotropic diffusion, where the diffusion length of the Sm atoms in the $[-1\ 5]$ direction is small, while the diffusion length in the $[N1]$ direction is large. Evidence of strongly anisotropic diffusion on a hexagonally reconstructed surface has been observed both in the Au on Au(100) system[29] and in the Pt on Pt(100) system.[30]

Bearing in mind the size of and the separation between the islands at the early stage (Fig. 7, Fig. 9), one recognizes that the Sm atoms that arrive on the surface must have a substantial surface mobility. Sm atoms, or possibly small clusters, are able to diffuse distances up to at least 100 Å on the surface, before reaching their final position and state. The large number of atoms in the elongated islands reflect a situation where the probability for a Sm atom to add to an already existing island is larger than starting the nucleation of a new Sm-Pt island.

From initial adsorption to several monolayers of Sm deposition, the photoemission and LEED data indicate that Sm and Pt form an intermixed, disordered phase in the surface. The island structure observed in the STM measurements must be regarded as a disordered Sm/Pt intermetallic

phase, where Sm and Pt have reacted and the reconstruction has been lifted thereby. Accompanying this lifting is a restructuring process due to the ''extra'' Pt atoms. The mixing between Sm and Pt continues for several monolayers of Sm deposition on the surface, and this process is probably gradually terminated by transport limitations in the developing intermetallic film. During the formation of the first monolayer, the observed island structure is not seen to influence the valence state of Sm; all Sm positions in the first monolayer yield Sm in its 3+ valence state.

CONCLUSION

When Sm is deposited onto a Pt(100)-hex-$R0.7°$ single-crystal surface, a surface intermetallic compound is argued to form. Pt(100) was exposed to Sm coverages in the range 0.3–20 Å. For all coverages, trivalent Sm was observed. Some divalent Sm was seen after ~20 Å Sm deposition, and was believed to stem from Sm atoms at the surface. STM shows that the first monolayer of the compound grows as long (100–1000 Å), narrow islands directed along the $[N\ 1]$ axis of the reconstruction. Sm adsorption induces a local lifting of the hexagonal reconstruction. The islands are seen to be centered on the elevated ridges of the reconstruction. Both anisotropic diffusion and a strongly directional activation energy for lifting the hexagonal surface reconstruction may contribute to the observed island shape.

ACKNOWLEDGMENTS

The financial support from the Norwegian Research Council is gratefully acknowledged. H.J.V. is indebted to Statoil, Norway for support from the VISTA programme. C.B. wishes to thank the Norwegian Research Council for a fellowship. We are grateful to the MAX-lab staff for very competent assistance. MAX-lab is supported by the Swedish Natural Science Research Council.

[1] See, e.g., J. M. Lawrence, P. S. Riseborough, and R. D. Parks, Rep. Prog. Phys. **44**, 1 (1981).
[2] G. K. Wertheim and G. Crecelius, Phys. Rev. Lett. **40**, 813 (1978).
[3] B. Johansson, Phys. Rev. B **19**, 6615 (1979).
[4] R. B. Schwarz and W. L. Johnson, Phys. Rev. Lett. **51**, 415 (1983).
[5] F. U. Hillebrecht, M. Ronay, D. Rieger, and F. J. Himpsel, Phys. Rev. B **34**, 5377 (1986).
[6] See, e.g., S. Raaen, C. Berg, and N. A. Braaten, Surf. Sci. **269/270**, 953 (1992), and references cited therein.
[7] D. M. Wieliczka and C. G. Olson, J. Vac. Sci. Technol. A **8**, 891 (1990).
[8] D. M. Jaffey, A. J. Gellman, and R. M. Lambert, Surf. Sci. **214**, 407 (1989).
[9] E. Beaurepaire, B. Carrière, P. Légaré, G. Krill, C. Brouder, D. Chandesris, and J. Lecante, Surf. Sci. **211/212**, 448 (1989).
[10] F. Bertran, T. Gourieux, G. Krill, M. F. Ravet-Krill, M. Alnot, J. J. Ehrhardt, and W. Felsch, Phys. Rev. B **46**, 7829 (1992).
[11] J. Tang, J. M. Lawrence, and J. C. Hemminger, Phys. Rev. B **47**, 16 477 (1993); **48**, 15 342 (1993).
[12] M. P. Dariel, in *Handbook on the Physics and Chemistry of Rare Earths*, edited by K. A. Gschneidner, Jr. and L. R. Eyring (North-Holland, Amsterdam, 1978), Vol. 1.
[13] Å. Fäldt and H. P. Myers, Phys. Rev. B **30**, 5481 (1984); **34**, 6675 (1986); **33**, 1424 (1986); Solid State Commun. **48**, 253 (1983); Phys. Rev. Lett. **52**, 1315 (1984).
[14] J. N. Andersen, I. Chorkendorff, J. Onsgaard, J. Ghijsen, R. L. Johnson, and F. Grey, Phys. Rev. B **37**, 4809 (1988).
[15] M. L. denBoer, C. L. Chang, S. Horn, and V. Murgai, Phys. Rev. B **37**, 6605 (1988).
[16] L. Tao, E. Goering, S. Horn, and M. L. den Boer, Phys. Rev. B **48**, 15 289 (1993).
[17] Å. Fäldt, D. K. Kristensen, and H. P. Myers, Phys. Rev. B **37**, 2682 (1988).
[18] P. Dubot, E. Alleno, M.-G. Barthés-Labrousse, C. Binns, C. Nicklin, C. Norris, and D. Ravot, Surf. Sci. **282**, 1 (1993).
[19] G. M. Roe, C. M. C. de Castilho, and R. M. Lambert, Surf. Sci. **301**, 39 (1994).
[20] B. Jørgensen, M. Christiansen, and J. Onsgaard, Surf. Sci. **251/252**, 519 (1991).
[21] C. Wigren, J. N. Andersen, R. Nyholm, M. Göthelid, M. Hammar, C. Törnevik, and U. O. Karlsson, Phys. Rev. B **48**, 11 014 (1993).
[22] C. Laubschat, G. Kaindl, W. D. Schneider, B. Reihl, and N. Mårtensson, Phys. Rev. B **33**, 6675 (1986); B. Johansson and N. Mårtensson, in *Handbook on the Physics and Chemistry of Rare Earths*, edited by K. A. Gschneidner, Jr., L. R. Eyring, and S. Hüfner (North-Holland, Amsterdam, 1987), Vol. 10.
[23] See, e.g., G. A. Somorjai, *Introduction to Surface Chemistry and Catalysis* (Wiley, New York, 1993), and references cited therein.
[24] D. G. Fedak and N. A. Gjostein, Surf. Sci. **8**, 77 (1967).
[25] M. A. Van Hove, R. J. Koestner, P. C. Stair, J. P. Biberian, L. L. Kesmodel, I. Bartos, and G. A. Somorjai, Surf. Sci. **103**, 189 (1981).
[26] W. Moritz, Habilitationsschrift, Ludwig-Maximilians-Universität, München, 1983.
[27] P. Heilmann, K. Heinz, and K. Müller, Surf. Sci. **83**, 487 (1979).
[28] D. Gibbs, B. M. Ocko, D. M. Zehner, and S. G. J. Mochrie, Phys. Rev. B **42**, 7330 (1990).
[29] S. Günther, E. Kopatzki, M. C. Bartelt, J. W. Evans, and R. J. Behm, Phys. Rev. Lett. **73**, 553 (1994).
[30] T. R. Linderoth, J. J. Mortensen, K. W. Jacobsen, E. Lægsgaard, I. Stensgaard, and F. Besenbacher (unpublished).
[31] A. Borg, A.-M. Hilmen, and E. Bergene, Surf. Sci. **306**, 10 (1994).
[32] M. P. Seah and W. A. Dench, Surf. Interface Anal. **1**, 2 (1979).
[33] H. J. Venvik, C. Berg, A. Borg, and S. Raaen (unpublished).
[34] C. Boeglin, B. Carrière, J. P. Deville, F. Scheurer, C. Guillot, and N. Barrett, Phys. Rev. B **45**, 3834 (1992).
[35] R. C. Baetzold, G. Apai, E. Shustorovich, and R. Jaeger, Phys. Rev. B **26**, 4022 (1982).
[36] P. Heimann, J. F. van der Veen, and D. E. Eastman, Solid State Commun. **38**, 595 (1981).

[37] K. Dückers and H. P. Bonzel, Europhys. Lett. **7**, 371 (1987).
[38] J. F. van der Veen, F. J. Himpsel, and D. E. Eastman, Phys. Rev. Lett. **44**, 189 (1980).
[39] F. Gerken, J. Barth, and C. Kunz, in *X-Ray and Atomic Inner-Shell Physics*, Proceedings of the International Conference on X-Ray and Atomic-Inner Shell Physics—1982, edited by B. Crasemann, AIP Conf. Proc. No. 94 (AIP, New York, 1982).
[40] See, e.g., *Binary Alloy Phase Diagrams*, 2nd ed., edited by T. B. Massalski, H. Okamoto, P. Subramanian, and L. Kacprzak (ASM International, Metals Park, OH, 1990), Vol. 3.
[41] J. Majerus, N. J. Castellani, and P. Légaré, Surf. Sci. **311**, L661 (1994).
[42] R. Q. Hwang, C. Günther, J. Schröder, S. Günther, E. Kopatzki, and R. J. Behm, J. Vac. Sci. Technol. A **10**, 1970 (1992).